STUDIES OF A HIGH TEMPERATURE CO-O_2 FUEL-TYPE CELL

by

LESLIE GUTIERREZ

B.S. Sioux Falls College, 1966

A MASTER'S THESIS

submitted in partial fulfillment of the

requirements for the degree

MASTER OF SCIENCE

Department of Chemistry

KANSAS STATE UNIVERSITY
Manhattan, Kansas

1969

Approved by:

James L. Copeland
Major Professor

TABLE OF CONTENTS

LIST OF FIGURES

LIST OF TABLES

LIST OF SYMBOLS

T	temperature in °K
E_T	emf at some temperature T
E_T°	standard emf at some temperature T
ΔG_T	Gibbs free energy change at some temperature T
ΔG_T°	standard Gibbs free energy change at some temperature T
ΔS	entropy change
ΔS°	standard entropy change
ΔH_T	enthalpy change at some temperature T
ΔH_T°	standard enthalpy change at some temperature T
K	equilibrium constant
R	gas constant
n	number of faradays passed
F	Faraday constant
C_p	molar heat capacity at constant pressure
ΔC_p	molar heat capacity difference of products and reactant
$(dE/dT)_p$	emf-temperature coefficient at constant pressure
P_{CO_2}	partial pressure of carbon dioxide
P_{CO}	partial pressure of carbon monoxide
P_{O_2}	partial pressure of oxygen
I	constant of integration
H_I	constant of integration
i	electric current
r	electrical resistance
p	electric power

INTRODUCTION AND THEORY

I. Purpose of Investigation

In recent years, attempts have been made to study electrochemical cells with molten salt electrolytes (1-4) in which the net chemical reaction represents only the consumption of oxygen and carbon and the formation of carbon dioxide. Such cells as these could have significance in two areas. First, these cells could be used to determine electrochemically the thermodynamic functions associated with the high temperature formation of carbon dioxide. Second, these cells could have fundamental importance in fuel cell research.

Unfortunately, such studies have met with limited success because of either the irreversible behavior of the electrode system or the inherent mechanical problems associated with the high corrosive nature of most electrolytic melts at operational temperatures.

It had been assumed that emf data could be obtained very near the theoretical value if one could obtain a suitable electrolytic system compatible with the structure of the cell container, and alter some previous procedures. This, in turn, would enable calculation of the thermodynamic properties of high temperature formation of carbon dioxide nearer their theoretical values. It was in light of this assumption, after having established the apparent stability of Vycor with molten polyphosphates, that this work has resulted.

The purpose of this investigation has been to extend these previous studies using a molten polyphosphate system as the electrolyte and carbon monoxide, rather than carbon, as the reductant. This work involves the study of the electrochemical oxidation of carbon monoxide at high temperatures and includes (a) emf measurements as a function of the temperature from 650° to 750°, (b) emf measurements as a function of various partial pressure ratios of

carbon dioxide to carbon monoxide, as determined by flowmeters, (c) calculation of high temperature thermodynamic functions associated with the formation of carbon dioxide from carbon monoxide, (d) interpretation of the results and some discussion of the possibilities of this system as a potential fuel cell.

II. Fuel Cells and Historical Background

In a general sense, a fuel cell may be defined as a galvanic cell in which the free energy of a fuel and an oxidizing agent are converted to electrical energy (5). The term "fuel" is interpreted rather liberally and is taken to include hydrogen. Oxygen is generally used as the oxidizing agent, although air has been employed. Ideally, both electrodes should be unaffected by the reaction, as should the electrolyte which separates them. At the "fuel" electrode (anode) of a fuel cell, the fuel is oxidized and electrons are released to the external circuit. Correspondingly, at the oxygen electrode (cathode) the electrons are accepted from the external circuit and the oxygen is reduced. The net cell reaction is then represented by the oxidation of the fuel.

Historically, these essential features which are presently ascribed to fuel cells were first incorporated in a device described by Grove (6) as early as 1839. His experiments describe the generation of electricity produced by supplying hydrogen and oxygen to two separate platinum electrodes immersed in sulfuric acid. It is known now that in this cell hydrogen was ionized at the anode, releasing electrons to the external circuit, and that the hydrogen ions were then effectively transported through the sulfuric acid electrolyte to the oxygen (cathode) electrode. There they reacted with hydroxyl ions formed by a reaction between oxygen, water, and electrons. The electrons, in traversing the external circuit, gave rise to an electric current.

Following Grove's original experiments, fuel cell research followed two

different lines. One was to oxidize the fuel (carbon) directly in a fuel cell. The other was to convert the available fuel, then coal, to hydrogen by the water gas process and use the hydrogen in a hydrogen-oxygen (air) cell.

In 1855 Becquerel (6) attempted to make a fuel cell which consumed carbon directly. A fused "nitre" retained in a platinum vessel served as the electrolyte, and a current was obtained between a carbon rod immersed in the electrolyte and the platinum. Jablockoff (7) made a similar cell using cast iron as the retaining vessel. However, both of these cells proved unsound in principle since the carbon was attacked by the fused nitrate mainly in a manner which produced no current. Jacques (8) extended the concept of a fused electrolyte when he designed and built a 1.5-kilowatt battery of fuel cells. Each cell consisted of an iron vessel containing fused sodium hydroxide into which was placed a carbon rod. Air was bubbled through the fused electrolyte, and current was drawn between the iron vessel and the carbon rod. Haber and Brunner (9) later showed that this was not a true carbon-oxygen fuel cell since hydrogen was being produced at the carbon electrode by the reaction of carbon with sodium hydroxide. Hydrogen was being oxidized electrolytically at the carbon electrode, which presumably contained some impurities which catalyzed the electrode reaction. It was further found that traces of manganese were essential to the operation of the cell, and that the manganese was oxidized to manganate by the air bubbled through the fused electrolyte. Since the electrolyte was not invariant, the Jacques cell was not a fuel cell.

Reed (10) in 1918 substituted borax containing manganese dioxide for the fused sodium hydroxide of the Jacques cell, and gold for the containing vessel. Air was not bubbled through the electrolyte, and in all probability manganese dioxide was the reactant at the cathode.

Baur, Brunner, and Pries (11, 12) who were primarily responsible for the

majority of carbon-consuming fuel cell research prior to the second world war, used solid electrolytes of zirconia stabilized with magnesia or ytteria. Although these electrolytes proved to be remarkably stable, the system was handicapped by the high temperatures (1050°) of operation.

Unfortunately many of the intrinsic problems associated with direct carbon-consuming fuel cells still persist today. High temperatures are a prerequisite if the oxidation of carbon is to proceed at a more than negligible rate. This, in turn, affects the efficiency and lifetime of the cell. In addition, at high temperatures where a reasonable reaction rate is obtained much of the fuel electrode could be consumed by carbon dioxide (the product of the electrode reaction) through the reaction

$$C + CO_2 \rightarrow 2CO \qquad 1.$$

This latter reaction does not contribute to the electrical energy of the cell and represents an additional loss in efficiency. These problems represent just a few of those which have made carbon-consuming fuel cells unattractive for commercial development.

Alternately, because of the difficulties associated with carbon-consuming fuel cells, many workers pursued the effort by using hydrogen or carbon monoxide as the fuel. In 1889 Mond and Langer (13) built a hydrogen-oxygen fuel battery consisting of platinum sheets as electrodes and dilute sulfuric acid as the electrolyte. Although the cell was expensive and the output low, it apparently represented the first fuel cell to provide measureable power under reasonably invariant conditions. Other hydrogen-oxygen fuel cell studies that followed were basically empirical in their approach and their success were limited. Various procedures and types of electrolytes, including binary mixtures of alkali halides (14), were employed but the fuel cells invariably yielded poor performances.

In 1939 Greger (15) proposed the first fuel cell reaction scheme for a fused salt (carbonate) electrolyte for an invariant system. He proposed that carbon dioxide and oxygen could be fed to and reacted at the "air" electrode to form carbonate ions

$$2CO_2 + O_2 + 4e^- \rightarrow 2CO_3^{-2} \qquad 2.$$

These ions would transport the charge through the electrolyte and be discharged at the fuel electrode, where they could react with either hydrogen or carbon monoxide

$$H_2 + CO_3^{-2} \rightarrow H_2O + CO_2 + 2e^- \qquad 3a.$$

$$CO + CO_3^{-2} \rightarrow 2CO_2 + 2e^- \qquad 3b.$$

As was mentioned, the majority of the fuel cell research was approached rather empirically up to this point, and no clear account of the supposed mechanism of the electrode reaction was understood. This subsequently led to research on "redox" fuel cells, where the problem of making the fuel and the oxygen react directly at the electrodes was avoided. Unfortunately, such studies of "redox" fuel cells (16, 17, 18) again proceeded with rather limited success.

Although what has been given here represents only a small fraction of the historical background of fuel cells, it should be mentioned that by the 1930's most of the potential fuel cell systems had been outlined in principle. However, up to this time, there had been no real attempt to engineer a useful power unit. In 1932 Bacon began building a useful power source based on a simple hydrogen-oxygen cell, and in 1959 (19) demonstrated a 5-kilowatt hydrogen-oxygen fuel cell battery. Through this effort much of the current wave of interest in fuel cell research was undoubtedly stimulated.

III. Thermodynamic Considerations

There are various methods of obtaining thermodynamic functions accompanying any chemical process (20, 21). Undoubtedly one of the most simple,

accurate, and complete methods of obtaining these functions is from emf data.

It can readily be shown that the decrease in Gibbs free energy accompanying any process at constant temperature and pressure is equal to the maximum reversible work, obtainable from that process, other than the work of expansion. If a particular reaction can be carried out in such a manner that, apart from the work of expansion, all the work is electrical, then the free energy will be equal in magnitude to the electrical work. Fortunately, many processes can be carried out reversibly in a galvanic cell and the maximum emf of the cell may be used to calculate the free energy change.

As mentioned, the cell must be operating reversibly before the emf can be used to calculate the free energy change of the reaction. The reversible emf of the cell may be determined in the following manner. When a cell is connected to an external source of emf, which is adjusted to balance exactly the emf of the cell, no current will flow and hence no net chemical change should be occurring in the cell. If the external emf is decreased by an infinitesimally small amount, current will flow from the cell and a chemical change, proportional to the quantity of current passing, should take place. On the other hand, current should flow in the opposite direction if the external emf is increased by a similar small amount, and the cell reaction should take place in the reverse direction (22). This method is referred to as potentiometry, and although it affords a way of measuring the reversible emf of a cell it by no means ensures that the electrode process is occurring reversibly. The ultimate condition is that the entire electrode process is virtually always in a state of equilibrium. This includes not only the charge-transfer process, but also any other activity (chemical or otherwise) pertinent to the electrode process. It may be mentioned that if large currents are allowed to flow through the cell when its emf is measured, polarization effects will arise within the cell. The

effect will be an observed emf less than the reversible emf (23).

Let us consider the following reaction,

$$CO(g) + (1/2)O_2(g) \rightarrow CO_2(g) \qquad 4.$$

If this oxidation can be carried out electrochemically and reversibly at constant temperature and pressure, the free energy change can be obtained directly from the observed emf of the cell by the use of eq 5

$$\Delta G = - nFE, \qquad 5.$$

where ΔG is the Gibbs free energy change of the reaction produced by the passage of n faradays of electricity through the cell, F is the Faraday constant, and E is the electromotive force of the cell. Analogously, if all substances represented by eq 4 are in their standard states, then

$$\Delta G^\circ = - nFE^\circ, \qquad 6.$$

where ΔG° and E° represent the standard free energy change and the standard electromotive force, respectively.

From the Gibbs free energy identity at constant temperature and pressure,

$$\Delta G = \Delta H - T\Delta S, \qquad 7.$$

where ΔH is the enthalpy change and ΔS is the entropy change accompanying the reaction, one can obtain

$$(d\Delta G/dT)_p = - \Delta S = (\Delta G - \Delta H)/T \qquad 8.$$

which, when combined with eq 5, leads to

$$\Delta S = nF(dE/dT)_p. \qquad 9.$$

The emf-temperature coefficient, $(dE/dT)_p$, in eq 9 can be readily obtained either from experimental data or by differentiating, with respect to temperature, an expression relating ΔG and the temperature. Experimentally, $(dE/dT)_p$ is obtained by plotting emf values *vs.* temperature and observing the slope of the curve at some one temperature.

Once having obtained ΔG and ΔS for a particular reaction, the enthalpy

change, ΔH, can be readily obtained by rearrangement of eq 7

$$\Delta H = \Delta G + T\Delta S. \qquad 10.$$

Thus, the thermodynamic functions ΔG, ΔH, and ΔS, as well as the equilibrium constant for a particular reaction, can be easily and simply determined from emf data.

An expression for the free energy change as a function of the temperature can be obtained by employing eq 7 and 8 with the help of differential calculus. Alternately, the two equations can be expressed as

$$d(\Delta G/T)/dT = - \Delta H/T^2, \qquad 11.$$

which would be suited for direct integration if ΔH were known as a function of the temperature. Such a function for ΔH involves heat capacity data for all substances involved in the particular reaction, as well as a ΔH value at some one temperature (usually 298°K).

Specifically, to obtain an expression for the free energy change as a function of the temperature for the reaction represented by eq 4, we first begin by expressing ΔH as a temperature function. The heat capacities at constant pressure, C_p, of CO_2, CO, and O_2 can ordinarily be represented by equations of the following algebraic type

$$C_p = a + bT + cT^{-2}, \qquad 12.$$

where a, b, and c are constants. The heat capacity difference of CO_2 and that of CO and O_2 can then be represented by

$$\Delta C_p = \Delta a + \Delta bT + \Delta cT^{-2} \qquad 13.$$

which allows eq 14 below to be integrated to yield an expression (eq 15) for ΔH as a function of the temperature,

$$(d\Delta H/dT)_p = \Delta C_p \qquad 14.$$

$$\Delta H = \Delta H_I + \Delta aT + (1/2)\Delta bT^2 - \Delta cT^{-1} \qquad 15.$$

ΔH_I is the constant of integration, and can be obtained by substituting a known

value of ΔH at some one temperature into eq 15 and solving for ΔH_I. Substitution of eq 15 into eq 11 and integrating yields,

$$\Delta G/T = \Delta H_I/T - \Delta a \ln T - (1/2)\Delta bT - (1/2)\Delta cT^{-2} + I \qquad 16.$$

or

$$\Delta G = \Delta H_I - \Delta aT \ln T - (1/2)\Delta bT^2 - (1/2)\Delta cT^{-1} + IT. \qquad 17.$$

The quantity I, another constant of integration, can be obtained in a similar manner used to obtain ΔH_I. Once the free energy change is obtained at any temperature, so also can the theoretical emf be obtained by means of eq 5. The emf-temperature coefficient is readily obtained by taking the derivative of eq 16 or 17 and solving the resulting expression at any particular temperature.

The free energy change is also related to the equilibrium constant K by

$$\Delta G = \Delta G^\circ + RT \ln K \qquad 18.$$

where R is the gas constant, $\ln K$ the natural logarithm of the equilibrium constant, and T the absolute temperature. When the system is in equilibrium $\Delta G = 0$ and

$$\Delta G^\circ = -RT \ln K \qquad 19.$$

This equation will be exact only if the equilibrium constant is expressed in terms of the activities of the reactants and products of the reaction. If the reaction involves only gases, then the standard state of unit activity may be replaced by a state of unit fugacity. At relatively low pressures the fugacity of a gas may be replaced by its equilibrium partial pressure without seriously affecting the value of the equilibrium constant (24).

IV. Electrolytic Systems

The cathode and anode reactions for the oxidation of carbon(graphite) to carbon dioxide in a molten, oxyanionic electrolyte may generally be written as

anode: $C(\text{graphite}) + 2[O^{-2}] = CO_2(g) + 4e^-$

cathode: $O_2(g) + 4e^- = 2[O^{-2}]$

net reaction: $C(graphite) + O_2(g) \rightarrow CO_2(g)$

where $[O^{-2}]$ represents some form of solvated oxide ion. In previous studies by Baur et al., (11, 12) an oxide was added to an appropriate melt to provide the oxide ion for the cell reaction. However, the oxide ion is potentially available from any oxyanion for which the corresponding oxide, or another form of the oxyanion exists. Some examples of such systems are the sulfate-sulfur trioxide system, the borate-boric oxide system and numerous others of similar nature.

In studies completed by Duke, et al., (1, 2) several molten salt (oxyanionic) electrolytes were employed in the electrochemical oxidation of carbon (graphite) to carbon dioxide. The proposed theoretical half-cell reactions with the sodium tungstate-tungstic anhydride system were as follow

anode: $C(graphite) + 2WO_4^{-2} \rightarrow CO_2(g) + 2WO_3 + 4e^-$

cathode: $2WO_3 + O_2(g) + 4e^- \rightarrow 2WO_4^{-2}$

net reaction: $C(graphite) + O_2(g) \rightarrow CO_2(g)$

Similarly, for the oxidation involving the sodium tetraborate-boric anhydride system the theoretical electrode reactions are

anode: $C(graphite) + 2B_4O_7^{-2} \rightarrow CO_2(g) + 4B_2O_3 + 4e^-$

cathode: $4B_2O_3 + O_2(g) + 4e^- \rightarrow 2B_4O_7^{-2}$

with the net reaction the same as before. Analogously, for the electrochemical oxidation of carbon monoxide one could propose similar electrode reactions. With a molten sodium polyphosphate system, using carbon monoxide as the reductant, the apparent theoretical electrode reactions are

anode: $CO(g) + P_2O_7^{-4} \rightarrow CO_2(g) + 2PO_3^{-1} + 2e^-$

cathode: $2PO_3^{-1} + (1/2)O_2(g) + 2e^- \rightarrow P_2O_7^{-4}$

net reaction: $CO(g) + (1/2)O_2(g) \rightarrow CO_2(g)$

EXPERIMENTAL

I. Chemicals

Reagent grade $NaPO_3$ and $Na_4P_2O_7 \cdot 10H_2O$ were obtained from the Baker and Adamson Company. The $Na_4P_2O_7 \cdot 10H_2O$ sample was dehydrated completely as possible in a porcelain casserole over a Fischer burner for approximately two hours. The sample, along with a separate sample of $NaPO_3$, was then transferred to an electric oven and dried a 130° for an additional 72 hours to remove any further trace of moisture. The samples were then allowed to cool in a desiccator before weighing into the Vycor cell container.

Carbon monoxide, 99.5% min. purity, C.P. grade, was obtained from the Matheson Gas Company. Oxygen, U.S.P. grade, and carbon dioxide, of unknown purity, were obtained from the Jayhawk Cylinder Gas Company. Both the carbon monoxide and dioxide were analyzed by mass spectrometer and found to be of high purity as expected for the carbon monoxide and assumed for the carbon dioxide. All gases were passed through separate drying tubes charged with $Mg(ClO_4)_2$ to ensure removal of any moisture prior to passage into the cell.

Reagent grade dibutyl phthalate was obtained from the Baker and Adamson Company, and was used without further purification as the manometric fluid in the constructed flowmeters.

II. Apparatus

A. Commercial Equipment

The electromotive force of the cell was determined with a Leeds and Northrup type K-3 potentiometer. A Leeds and Northrup Model No. 2420-c reflecting type galvanometer, whose light was activated by a 6-volt lead acid storage battery, served as null point indicator. An Eppley Laboratory, Inc., No. 761051 standard cell with a constant voltage of 1.01929 V at 22°, and four 1.5 V Eveready dry cells, arranged in parallel, served as the standard and

working cells, respectively.

The chromel-alumel thermocouple leads from the cell were silver soldered, and had a reference junction in an ice bath at 0°. A Leeds and Northrup Model No. 8691 millivolt potentiometer with an internal standard cell served to monitor the thermocouple emf in the cell (25).

A Heathkit VOM Model MM-1, and decade resistance box Model IN-11 were used to obtain the maximum constant current delivered by the cell with a minimum resistance load.

B. Constructed Equipment

The cell, shown in Fig.1, consisted of a U-shaped 17-mm O.D. Vycor tube with limbs 30 cm long (26). The latter terminated in standard tapered Vycor wall joints 24/40, which when in place extended upwards out of a vertical, cylindrical resistance furnace. A narrower 13-mm o.d. Vycor tube extended upward from the center of the U-cell to allow introduction of the chromel-alumel thermocouple junction. All three wells were commonly joined at the bottom of the cell so that the electrolytic melt could freely pass into all three.

Figure 1 also includes a sketch of the CO_2-CO and the O_2 gas electrodes. Vycor gas delivery tubes 6-mm o.d. extend 31 cm down from the ring seals in the outer Vycor ground joints. Vycor-Pyrex graded seals, 6-mm o.d., permit the upper portions of the electrodes to terminate in 6-mm o.d. Pyrex tubing. Platinum wires, 24-gauge, which served as electrical contacts and electrode substrates, were sealed into the Pyrex at the upper ends of the electrodes, and extended downward to within 1.5 cm of the ends of the delivery tubes. Small holes were placed 1.5 and 1.25 inches above the ends of the CO_2-CO electrode and O_2 electrode, respectively. This allowed the gases to escape from the gas delivery tubes without forcing the electrolytic melt out

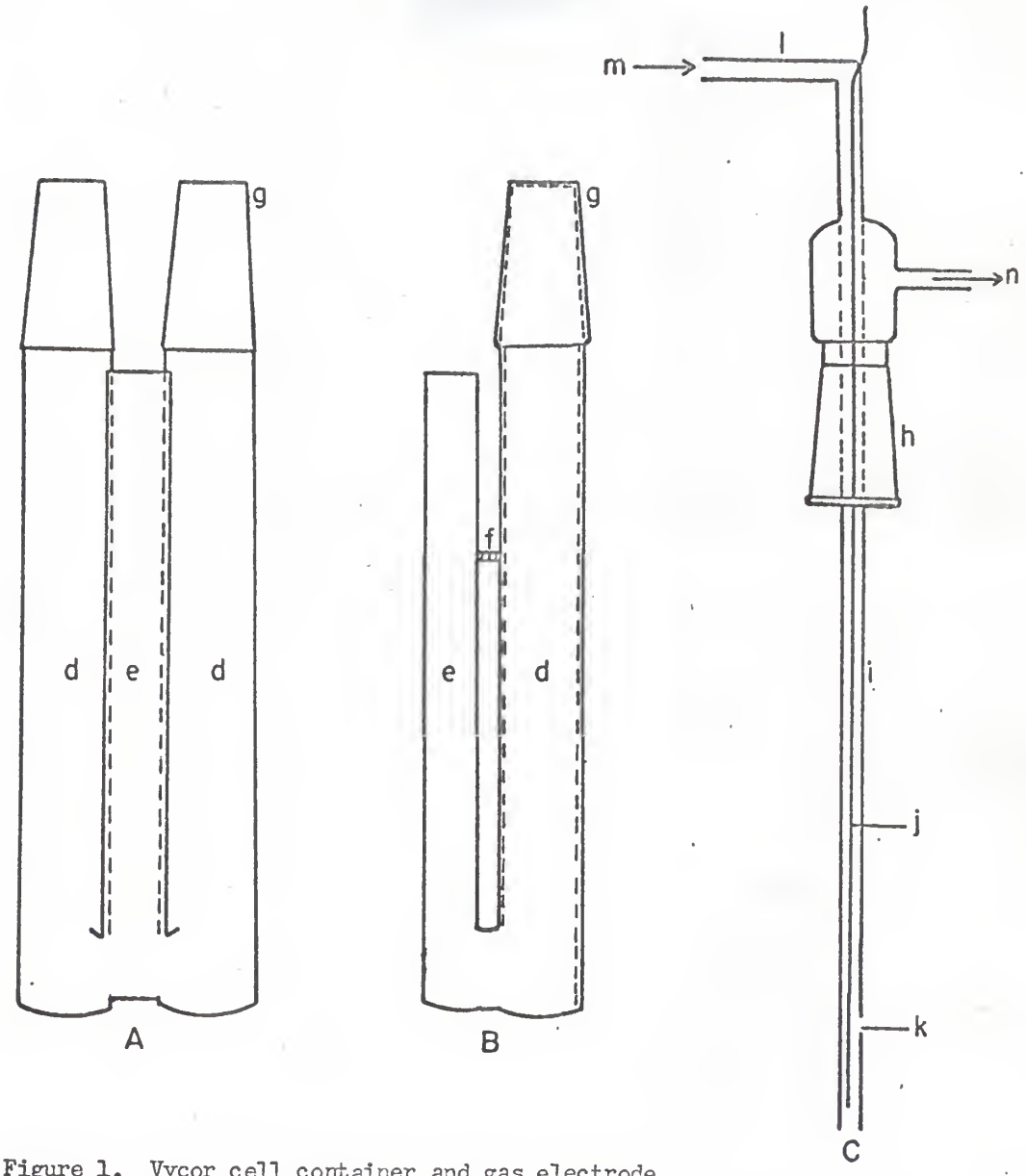

Figure 1. Vycor cell container and gas electrode.
Legend: A and B:front and side view of Vycor cell container, C:gas electrode, d:gas wells, e:thermocouple well, f:brace, g:inner Vycor ground joint, h:outer Vycor ground joint, i:gas delivery tube, j:Pt wire, k:gas exit orifice, l:Pyrex tube, m:gas inlet, n:gas outlet.

the ends of these tubes once the electrodes were in place.

Flowmeters, for determining the rates of flow of the gases, were constructed from 7-mm o.d. Pyrex tubing and Pyrex capillary tubing, 2-mm i.d. The Pyrex and capillary tubing, both U-shaped, were commonly jointed by two 7-mm o.d. Kimax T's, and Tygon tubing. These assemblies were then attached to meter sticks. A gas passes through the "T" on one side of the flowmeter, flows through the capillary, and exits through the "T" on the opposite side of the flowmeter. The lower Pyrex tubing is half-filled with dibutyl phthalate. As the gas flows through the capillary, a difference in the levels of the dibutyl phthalate in the two arms of the U-tube is observed. The greater the flow rate of the gas, the greater the differential height. The CO_2 and CO flowmeters were calibrated, using a gas buret, by observing the times required to displace certain volumes of dibutyl phthalate from the buret at several differential heights in the flowmeters.

The vertical, cylindrical furnace was constructed by S. Radak. It consisted of a 1/4-inch Transite top and bottom, and a 2-inch i.d. Norton Company aluminum oxide core, which was fixed vertically in the furnace housing. The outside of the core was wound with 18-gauge Chromel-A-wire. Norton Company Alundum No. RA 1055 refractory cement was placed over the outside of the wire-wound core. Super Stic-Tite asbestos cement served as insulation between the core and the walls of the furnace. Temperature in the furnace was maintained with a 220-volt Powerstat, and was monitored by a 0-5 amp a.c. ammeter.

III. Procedure

The cell container was thoroughly washed with dichromate cleaning solution, and was rinsed repeatedly with distilled water and finally with deionized water. The electrodes were first cleaned with hot, conc. HNO_3 and were then rinsed with distilled and deionized water. After the electrodes had dried,

and prior to placing them in the cell, the Pt wires, which would be in contact with the melt, were heated to a red glow with an oxygen torch to remove, by oxidation, any other contamination.

After the $NaPO_3$ and $NaP_2O_7 \cdot 10H_2O$ had been dehydrated and allowed to cool in the desiccator, 63.6500 g of $NaPO_3$ and 31.3500 g of $Na_4P_2O_7$ were weighed-out and thoroughly mixed. The mixture, corresponding to a composition of 33 wt. % of $Na_4P_2O_7$ and 67 wt. % of $NaPO_3$ and a eutectic point of about 575° (27), was then poured into the Vycor cell container and fused. The level of the fused electrolyte was fixed so that when the electrodes were in place the small gas exit orifice of the O_2 electrode was slightly below the level of the melt, and that of the CO_2-CO electrode was slightly above it. Thus, when the gases were allowed to flow, only the O_2 would bubble into the melt. The CO_2-CO gas mixture was not bubbled because of the difficulty in reading the flowmeters.

The gas flow system, from the respective gas cylinders to the cell, is shown schematically in Fig. 2. Tygon tubing was employed to deliver the gases from the cylinders to the cell. An O_2 regulator and a CO regulator were used on the respective cylinders, and a needle valve was employed on the CO_2 cylinder, to maintain small rates of flow to the cell as indicated by the flowmeters. The gases flowed from their respective cylinders through drying tubes charged with $Mg(ClO_4)_2$, then through the flowmeters, and finally into 250-ml Erlenmeyer flasks before flowing to their respective electrodes. The Erlenmeyer flasks served as traps to prevent any dibutyl phthalate in the flowmeters from flowing into the cell in the event of any sudden change in the rates of flow of the gases. The CO and CO_2 gases were mixed between their respective flowmeters and a 250-ml Erlenmeyer flask by means of a 7-mm o.d. Pyrex "Y" connector. Hence, the CO and CO_2 flow rates were determined by their flowmeters, and were then allowed to mix by means of the "Y" connector before the gas mixture passed

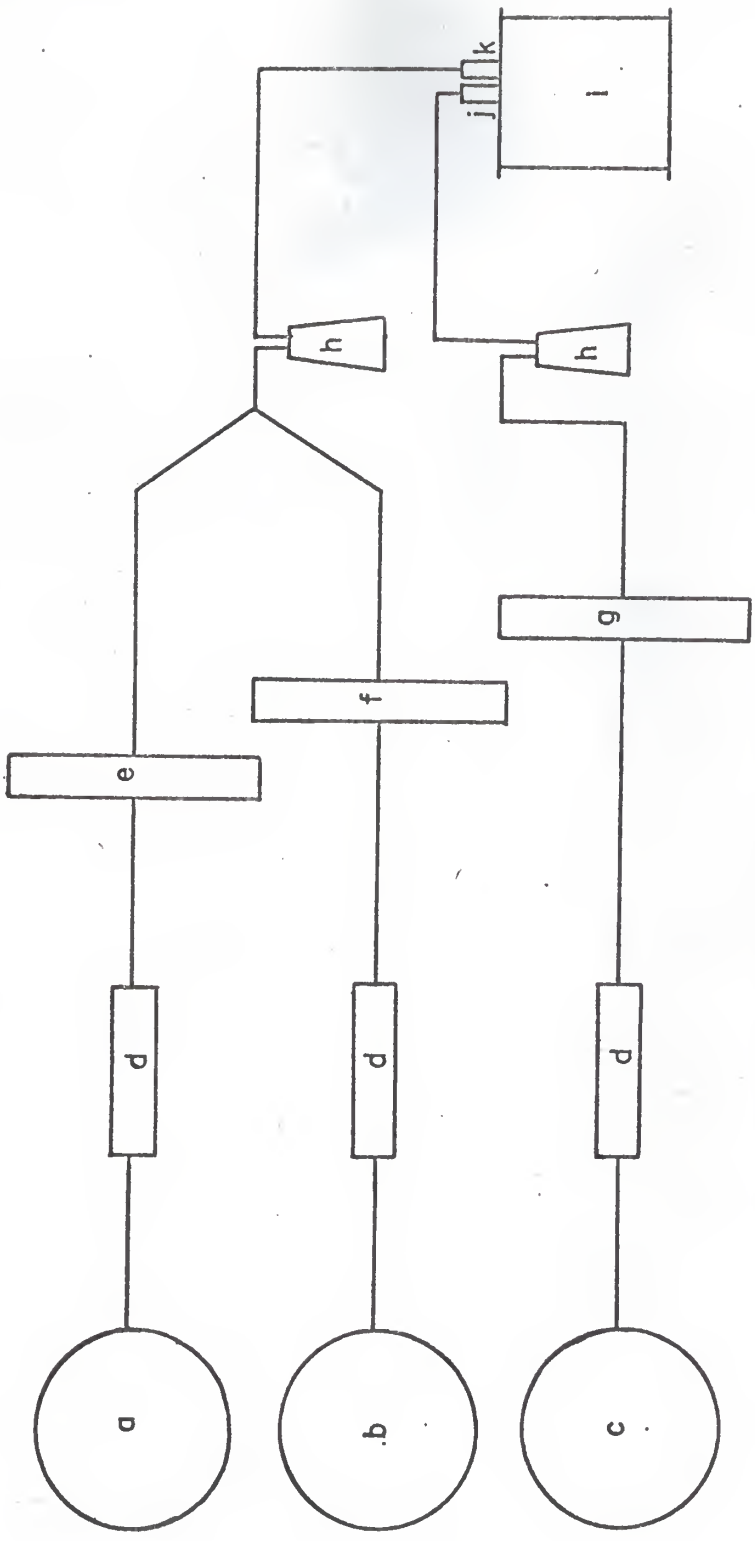

Figure 2. Gas flow system. Legend: a:CO gas cylinder, b:CO_2 gas cylinder, c:O_2 gas cylinder, d:$Mg(ClO_4)_2$ charged drying tubes, e:CO flowmeter, f:CO_2 flowmeter, g:O_2 flowmeter, h:250 ml Erlenmeyer flasks, j:O_2 electrode, k:CO_2-CO electrode, and l:furnace.

into the CO_2-CO electrode well.

Initially, only CO and O_2 were passed into the cell and allowed to react at 750° until some stability, as determined by the potentiometer, was achieved. As soon as this stability was achieved (after about 72 hours) the CO flow rate was increased to 1.00 cm^3 sec^{-1}, and the differential height in the O_2 flowmeter was set at about 0.75 cm. The reaction was allowed to equilibrate at these flow rates and at 750°. The emf was then determined from 750°, in intervals of 10 degrees, to 650° and from 650° back to 750° in intervals of 10 degrees. These readings were repeated until fairly reproducible values (± 1.5 mv) were obtained. This procedure was repeated for five different runs. Each run corresponded to a different flow rate ratio of CO_2 to CO, but the total rate of flow of CO_2 plus CO was always kept equal to 1.00 cm^3 sec^{-1}. In all these runs the differential height in the O_2 flowmeter was kept at about 0.75 cm. The CO_2 to CO flow rate ratios studied were 0.258, 0.656, 1.00, 3.17 and 9.00, in addition to the run involving pure CO.

In determining the maximum constant current at a minimum resistance load, the decade resistance box and VOM were placed in series with the cell. Only CO at a flow rate of 1.00 cm^3 sec^{-1}, and O_2 as indicated above flowed into the cell at 750°. The resistance was successively lowered until there appeared to be no decay in the current. The current delivered by the cell was recorded after maintaining a constant value of about 28 microamps into a load of $2.8 \cdot 10^4$ ohms for about 1/2 hour.

RESULTS AND CALCULATIONS

The theoretical standard free energy values for the oxidation of CO, eq 4, from 650° to 750° were calculated using eq 17. K. K. Kelly (28) expresses the appropriate ΔC_p as

$$\Delta C_p = 0.2 + 0.62\ 10^{-3}T - 1.75 \cdot 10^{5}T^{-2} \qquad 20.$$

where T is the absolute temperature. Eq 20 for ΔC_p is assumed valid to 2000°K. Integration of eq 11, using the above ΔC_p expression and ΔH_{298}° = -67,636 cal (28), allows one to express the standard enthalpy change, ΔH_T°, as a function of the temperature within the limits of ΔC_p, as

$$\Delta H_T^{\circ} = -68{,}310 + 0.2T + 0.31 \cdot 10^{-3}T^2 + 1.75 \cdot 10^{5}T^{-1} \qquad 21.$$

The standard free energy change as a function of the temperature, ΔG_T°, can then be expressed by the appropriate integration of eq 11

$$\Delta G_T^{\circ} = -68{,}310 - 0.2T\ln T - 0.31 \cdot 10^{-3}T^2 - 0.875 \cdot 10^{5}T^{-1} + IT \qquad 22.$$

The constant of integration, I, is 23.3 cal deg^{-1}, obtained by solving eq 22 with ΔG_{298}° = -61,452 cal (28).

The theoretical standard electromotive force, E_T°, at some temperature T is then readily obtained by combining eq 6 and 22. It should be emphasized that in all of the above expressions the temperature, T, is in absolute degrees.

A combination of eq 2, 3, and 15 leads directly to the Nernst equation which for the electrochemical oxidation of CO, eq 1, can written as

$$E_T = E_T^{\circ} - (RT/nF)\ln\left(P_{CO_2}/P_{CO} \cdot P_{O_2}^{1/2}\right) \qquad 23.$$

where E_T, E_T°, R, T, n, and F have their usual electrochemical designation as previously indicated. The natural logarithm, $\ln\left(P_{CO_2}/P_{CO} \cdot P_{O_2}^{1/2}\right)$, is expressed in terms of the partial pressures of CO_2, CO, and O_2 respectively.

The theoretical emf's of the cell from 650° to 750°, when the CO_2 to CO partial pressure ratio was not equal to unity, were obtained using eq 23.

Tables 1 to 5 summarize the emf-temperature studies for the electro-

chemical oxidation of CO with the common logarithms of the various partial pressure ratios of CO_2 to CO as indicated. For all these runs the oxygen partial pressure was taken as unity. The experimental emf values represent averages of several readings taken over periods of several hours. The individual readings were taken as the temperature was varied from 750° to 650°, and from 650° back to 750°, and were recorded when fairly reproducible values (±1.5 mv) were obtained. In addition, the theoretical emf values, as well as the experimental and theoretical emf-temperature coefficients, are included for comparison. Table 6 summarizes a similar treatment for the pure CO run with its flow rate at 1.00 cm^3 sec^{-1}.

Figure 3 is a graph of the five emf-temperature dependence plots with the common logarithms of the five different partial pressure ratios of CO_2 to CO as indicated. Also included is the emf-temperature plot of the pure CO run. The slopes were obtained from a least squares analysis and are included as the experimental emf-temperature coefficients in Tables 1 to 6.

Figure 4 depicts the relationship between the theoretical emf and the temperature with the common logarithms of the partial pressure ratios of CO_2 to CO as indicated.

As can be seen from the theoretical plots, the emf-temperature coefficients decrease (become more negative) as the partial pressure ratio of CO_2 to CO increases. This is as expected since as the CO_2 partial pressure increases the shift in the equilibrium will be in the direction which opposes the oxidation. A some what similar trend is indicated by the experimental emf-temperature coefficients.

Tables 7 to 11 summarize the experimental calculations of ΔG_T, ΔH_T, ΔS, and K (equilibrium constant) from 650° to 750° with the common logarithms of the CO_2 to CO partial pressure ratios as indicated. In addition, the corres-

ponding theoretical values are included for comparison. The theoretical and experimental free energy changes were obtained by substituting the appropiate emf's into eq 5. These values were then used to calculate the theoretical and experimental equilibrium constants by employing eq 19. The theoretical and experimental emf-temperature coefficients and eq 9 allows the entropy changes to be calculated. The enthalpy changes, at some one temperature, are subsequently found from the known free energy and entropy changes and the use of eq 10.

Figure 5 is a graph of the experimental emf vs. the common logarithms of the CO_2 to CO partial pressure ratios with the temperatures as indicated. The slopes again are least squares. However, the individual points are not included for the sake of avoiding confusion. The individual points are available for plotting from Tables 1 to 5.

Figure 6 represents a graph of the theoretical emf vs. the common logarithms of the CO_2 to CO partial pressure ratios with the temperatures as indicated.

Probable errors were calculated for ΔG, ΔS, and ΔH at 700° with the $\log (P_{CO_2}/P_{CO}) = -0.1831$ and were taken to be representative of the errors that would be obtained for the same functions at different temperatures and ratios of the CO_2 to CO partial pressures. The functions with the errors included are shown below,

$$\Delta G = -(45{,}578 \pm 55) \text{ cal}$$

$$\Delta S = -(15.3 \pm 0.1) \text{ e.u.}$$

$$\Delta H = -(60{,}565 \pm 114) \text{ cal}$$

The error in ΔS is the least squares probable error.

In comparing the experimental to the theoretical thermodynamic functions of Tables 7 to 11, it is seen that the best agreement is with the free energy

changes. Errors of about 10% from the theoretical values were found at the smallest CO_2 to CO partial pressure ratio, with a trend towards better agreement as the ratio increases. Obviously the same holds for the experimental and theoretical equilibrium constants. The deviation of the experimental from the theoretical is slightly higher (about 13%) for the enthalpy changes. However, there appears to be no trend towards better agreement as the CO_2 to CO partial pressure ratio varies. One interesting feature is that the enthalpy changes are rather constant from 650° to 750°, not only within a particular CO_2 to CO partial pressure ratio but also with varying ratios. A constant theoretical standard enthalpy change (± 1.5 cal) over a 100 degree temperature range (650° to 750°) is obtained when calculated from the Gibbs-Helmholtz equation. However, eq 21 predicts a change of about 55 cal over the same temperature range.

Table 12 summarizes the slopes of both the theoretical and the experimental emf *vs.* the common logarithm of the CO_2 to CO partial pressure ratios with the temperature as indicated. As can be seen the experimental slope deviates considerably from the theoretical slope (about 75 to 80%). However, the oxidation does appear to follow Nernstian behavior although the error is considerable.

An observed current of 28 microamps flowing under a load of $2.8 \cdot 10^4$ ohms allows the power generated by the cell to be calculated from

$$p = i^2 r \qquad 24.$$

where p is the power, i is the electrical current, and r is the resistance. The power of the cell at 750° was found to be $2.20 \cdot 10^{-5}$ watts.

Table 1. Summary of the emf-temperature dependence of the electrochemical oxidation of CO to CO_2, with the common logarithm of the CO_2 to CO partial pressure ratio equal to -0.5884.

Temp. (°C)	Experimental $\underline{E}$(V)	Theoretical $\underline{E}$(V)
650	1.00050	1.10375
660	0.99880	1.09969
670	0.99660	1.09571
680	0.99400	1.09167
690	0.99060	1.08765
700	0.98810	1.08361
710	0.98410	1.07963
720	0.98020	1.07560
730	0.97610	1.07159
740	0.97210	1.06757
750	0.96790	1.06357

Experimental $(d\underline{E}/d\underline{T})_p = -3.33 \cdot 10^{-4}$ V deg^{-1}

Theoretical $(d\underline{E}/d\underline{T})_p = -4.02 \cdot 10^{-4}$ V deg^{-1}

Table 2. Summary of the emf-temperature dependence of the electrochemical oxidation of CO to CO_2, with the common logarithm of the CO_2 to CO partial pressure ratio equal to -0.1831.

Temp. (°C)	Experimental $\underline{E}$(V)	Theoretical $\underline{E}$(V)
650	0.98679	1.06663
660	0.98338	1.06217
670	0.98017	1.05778
680	0.97702	1.05334
690	0.97323	1.04893
700	0.96996	1.04449
710	0.96699	1.04010
720	0.96394	1.03566
730	0.96081	1.03125
740	0.95770	1.02683
750	0.95435	1.02243

Experimental $(d\underline{E}/d\underline{T})_p = -3.24 \cdot 10^{-4}$ V deg^{-1}

Theoretical $(d\underline{E}/d\underline{T})_p = -4.42 \cdot 10^{-4}$ V deg^{-1}

Table 3. Summary of the standard emf-temperature dependence of the electrochemical oxidation of CO to CO_2.

Temp. (°C)	Experimental $\underline{E}°$(V)	Theoretical $\underline{E}°$(V)
650	0.98430	1.04986
660	0.98120	1.04522
670	0.97830	1.04065
680	0.97520	1.03603
690	0.97180	1.03143
700	0.96850	1.02681
710	0.96510	1.02224
720	0.96170	1.01762
730	0.95810	1.01303
740	0.95480	1.00843
750	0.95160	1.00385

Experimental $(d\underline{E}°/d\underline{T})_p = -3.31 \cdot 10^{-4}$ V deg^{-1}

Theoretical $(d\underline{E}°/d\underline{T})_p = -4.60 \cdot 10^{-4}$ V deg^{-1}

Table 4. Summary of the emf-temperature dependence of the electrochemical oxidation of CO to CO_2, with the common logarithm of the CO_2 to CO partial pressure ratio equal to 0.5011.

Temp. (°C)	Experimental $\underline{E}$(V)	Theoretical $\underline{E}$(V)
650	0.97750	1.00397
660	0.97400	0.99883
670	0.97082	0.99376
680	0.96740	0.98865
690	0.96393	0.98355
700	0.96040	0.97843
710	0.95700	0.97337
720	0.95345	0.96825
730	0.95003	0.96316
740	0.94660	0.95806
750	0.94295	0.95299

Experimental $(d\underline{E}/d\underline{T})_p = -3.46 \cdot 10^{-4}$ V deg^{-1}

Theoretical $(d\underline{E}/d\underline{T})_p = -5.10 \cdot 10^{-4}$ V deg^{-1}

Table 5. Summary of the emf-temperature dependence of the electrochemical oxidation of CO to CO_2, with the common logarithm of the CO_2 to CO partial pressure ratio equal to 0.9542.

Temp. (°C)	Experimental $\underline{E}$(V)	Theoretical $\underline{E}$(V)
650	0.96680	0.96247
660	0.96395	0.95689
670	0.96060	0.95137
680	0.95755	0.94580
690	0.95515	0.94026
700	0.95285	0.93469
710	0.95005	0.92918
720	0.94700	0.92360
730	0.94365	0.91807
740	0.94025	0.91252
750	0.93675	0.90700

Experimental $(d\underline{E}/d\underline{T})_p = -2.94 \cdot 10^{-4}$ V deg^{-1}

Theoretical $(d\underline{E}/d\underline{T})_p = -5.55 \cdot 10^{-4}$ V deg^{-1}

Table 6. Summary of the emf-temperature dependence for the run involving pure CO (flow rate = 1.00 cm^3 sec^{-1}).

Temp. (°C)	Experimental $\underline{E}$(V)
650	1.00940
660	1.00590
670	1.00290
680	0.99960
690	0.99620
700	0.99290
710	0.98990
720	0.98724
730	0.98390
740	0.98005
750	0.97629

Experimental $(d\underline{E}/d\underline{T})_p = -3.25 \cdot 10^{-4}$ V deg^{-1}

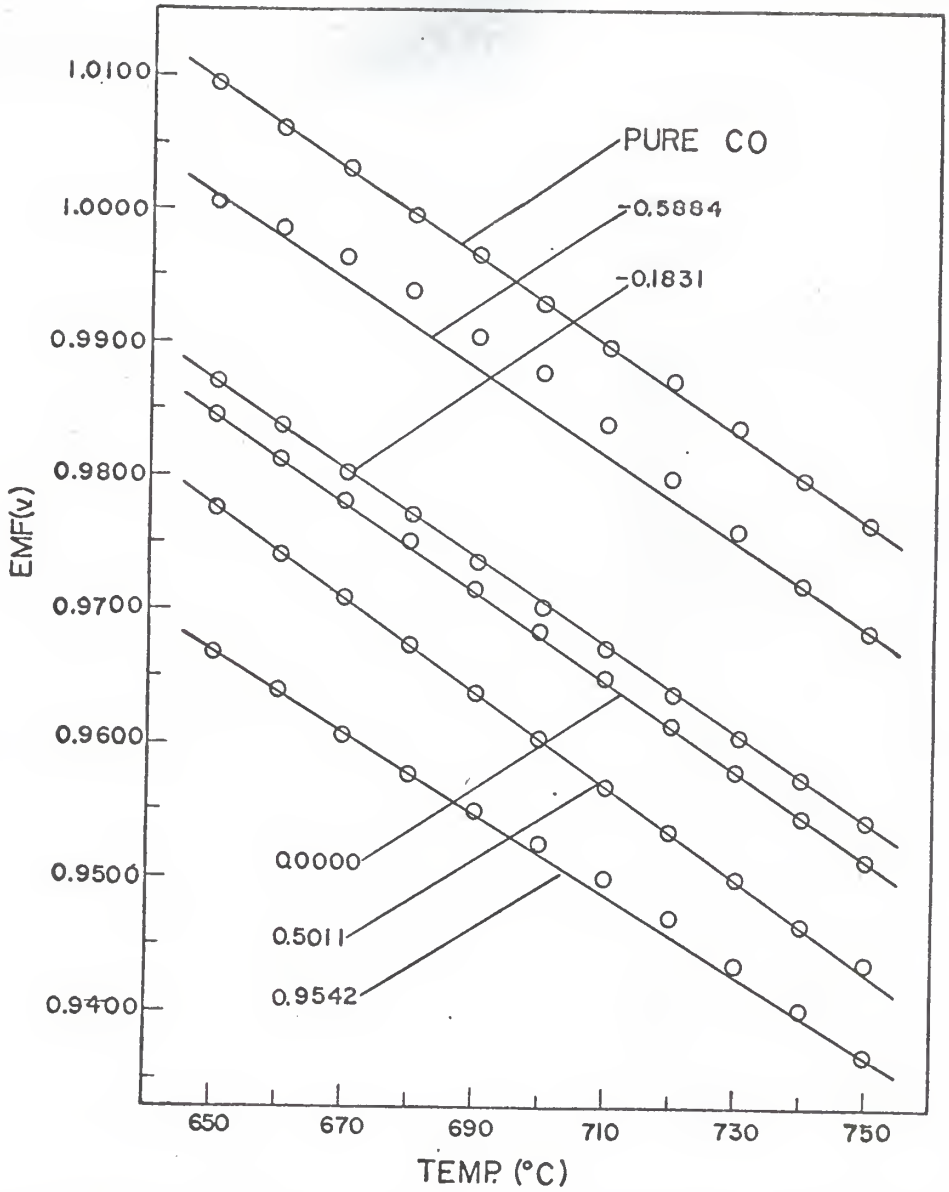

Figure 3. Experimental emf vs. temperature, with the common logarithm of the CO_2 to CO partial pressure ratios as indicated.

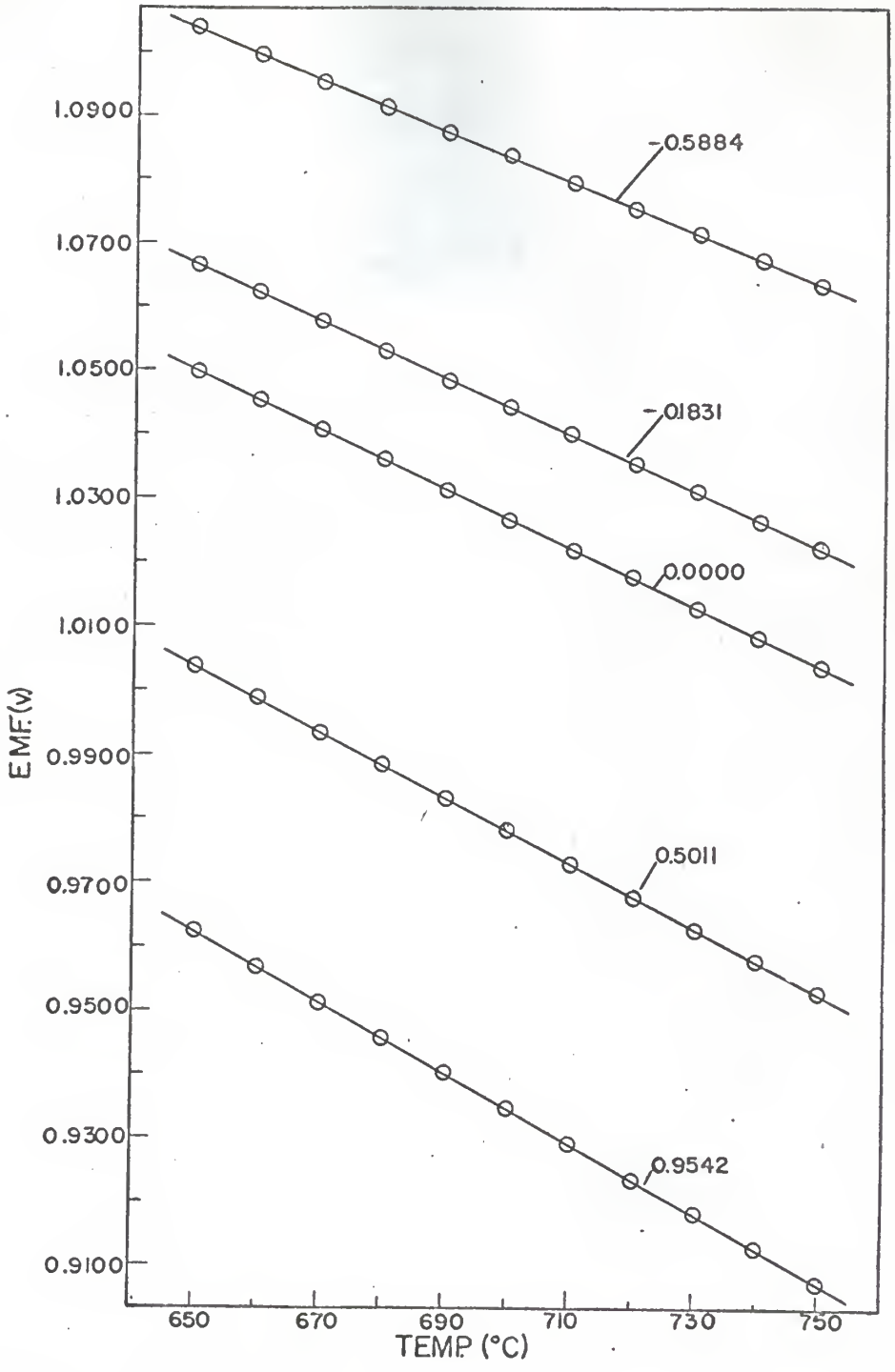

Figure 4. Theoretical emf *vs.* temperature, with the common logarithm of the CO_2 to CO partial pressure ratios as indicated.

Table 7. Summary of high temperature thermodynamic functions of CO_2 formation, with log (P_{CO_2}/P_{CO}) = -0.5884.

ΔS^a = -15.4 e.u. ΔS^b = -18.5 e.u.

T (°K)	$-\Delta G_T^a$ (cal)	$-\Delta G_T^b$ (cal)	$-\Delta H_T^a$ (cal)	$-\Delta H_T^b$ (cal)	$^aK \cdot 10^{-10}$	$^bK \cdot 10^{-11}$
923.15	46,148	50,910	60,365	67,988	8.51	11.2
933.15	46,069	50,723	60,440	67,986	6.17	7.59
943.15	45,968	50,539	60,493	67,987	4.47	5.13
953.15	45,848	50,353	60,527	67,986	3.24	3.55
963.15	45,691	50,167	60,524	67,985	2.34	2.40
973.15	45,578	49,981	60,565	67,984	1.74	1.66
983.15	45,391	49,798	60,532	67,986	1.23	1.18
993.15	45,211	49,612	60,506	67,985	0.891	0.832
1003.15	45,022	49,427	60,471	67,985	0.632	0.589
1013.15	44,838	49,241	60,441	67,984	0.470	0.417
1023.15	44,644	49,057	60,401	67,985	0.343	0.302

a = experimental values
b = theoretical values

Table 8. Summary of high temperature thermodynamic functions of CO_2 formation, with $\log (P_{CO_2}/P_{CO}) = -0.1831$.

$\Delta S^a = -14.9$ e.u. $\Delta S^b = -20.4$ e.u.

T (°K)	$-\Delta G_T^a$ (cal)	$-\Delta G_T^b$ (cal)	$-\Delta H_T^a$ (cal)	$-\Delta H_T^b$ (cal)	$^aK \cdot 10^{-10}$	$^bK \cdot 10^{-11}$
923.15	45,515	49,198	59,270	68,030	6.03	4.47
933.15	45,358	48,992	59,262	68,028	4.17	2.95
943.15	45,210	48,790	59,263	68,030	2.95	2.00
953.15	45,065	48,585	59,267	68,029	2.14	1.38
963.15	44,890	48,381	59,241	68,029	1.55	0.995
973.15	44,739	48,177	59,239	68,029	1.12	0.661
983.15	44,602	47,974	59,251	68,030	0.820	0.457
993.15	44,461	47,769	59,259	68,029	0.610	0.324
1003.15	44,317	47,566	59,264	68,030	0.452	0.229
1013.15	44,174	47,362	59,270	68,030	0.337	0.166
1023.15	44,019	47,159	59,264	68,031	0.264	0.118

a = experimental values
b = theoretical values

Table 9. Summary of standard high temperature thermodynamic functions of CO_2 formation.

$\Delta S^{\circ a} = -15.3$ e.u. $\Delta S^{\circ b} = -21.2$ e.u.

T (°K)	$-\Delta G_T^{\circ a}$ (cal)	$-\Delta G_T^{\circ b}$ (cal)	$-\Delta H_T^{\circ a}$ (cal)	$-\Delta H_T^{\circ b}$ (cal)	$^aK \cdot 10^{-10}$	$^bK \cdot 10^{-11}$
923.15	45,400	48,424	59,524	67,995	5.62	2.88
933.15	45,257	48,210	59,534	67,993	3.98	1.95
943.15	45,124	48,000	59,554	67,995	2.88	1.32
953.15	44,981	47,786	59,564	67,993	2.04	0.912
963.15	44,824	47,574	59,560	67,993	1.48	0.631
973.15	44,672	47,361	59,561	67,992	1.07	0.437
983.15	44,515	47,150	59,557	67,993	0.783	0.302
993.15	44,358	46,937	59,553	67,992	0.578	0.214
1003.15	44,192	46,726	59,540	67,993	0.425	0.151
1013.15	44,040	46,513	59,541	67,992	0.316	0.107
1023.15	43,892	46,302	59,546	67,993	0.237	0.077

a = experimental values
b = theoretical values

Table 10. Summary of high temperature thermodynamic functions of CO_2 formation, with log (P_{CO_2}/P_{CO}) = 0.5011.

ΔS^a = -16.0 e.u. ΔS^b = -23.5 e.u.

T (°K)	$-\Delta G_T{}^a$ (cal)	$-\Delta G_T{}^b$ (cal)	$-\Delta H_T{}^a$ (cal)	$-\Delta H_T{}^b$ (cal)	$^aK \cdot 10^{-10}$	$^bK \cdot 10^{-10}$
923.15	45,087	46,308	59,857	68,002	4.68	9.12
933.15	44,925	46,071	59,855	68,000	3.31	6.17
943.15	44,779	45,837	59,869	68,001	2.40	4.17
953.15	44,621	45,601	59,871	68,000	1.70	2.88
963.15	44,461	45,366	59,871	68,000	1.23	1.95
973.15	44,298	45,130	59,868	68,000	0.887	1.35
983.15	44,141	44,896	59,871	68,000	0.647	0.953
993.15	43,977	44,660	59,867	67,999	0.476	0.673
1003.15	43,820	44,425	59,870	67,999	0.352	0.478
1013.15	43,662	44,190	59,872	67,999	0.262	0.340
1023.15	43,493	43,956	59,863	68,000	0.195	0.244

a = experimental values
b = theoretical values

Table 11. Summary of high temperature thermodynamic functions of CO_2 formation, with log $(P_{CO_2}/P_{CO}) = 0.9542$.

$\Delta S^a = -13.6$ e.u. $\Delta S^b = -26.5$ e.u.

T (°K)	$-\Delta G_T^a$ (cal)	$-\Delta G_T^b$ (cal)	$-\Delta H_T^a$ (cal)	$-\Delta H_T^b$ (cal)	$^aK \cdot 10^{-10}$	$^bK \cdot 10^{-10}$
923.15	44,593	44,394	57,148	68,027	3.63	3.24
933.15	44,462	44,136	57,153	68,025	2.57	2.19
943.15	44,307	43,882	57,134	68,027	1.86	1.48
953.15	44,167	43,625	57,130	68,026	1.35	1.00
963.15	44,056	43,369	57,155	68,026	0.993	0.693
973.15	43,950	43,112	57,185	68,025	0.741	0.481
983.15	43,821	42,858	57,192	68,027	0.550	0.336
993.15	43,680	42,601	57,187	68,026	0.409	0.235
1003.15	43,525	42,346	57,168	68,027	0.304	0.168
1013.15	43,369	42,090	57,148	68,027	0.226	0.120
1023.15	43,207	41,835	57,122	68,028	0.169	0.086

a = experimental values
b = theoretical values

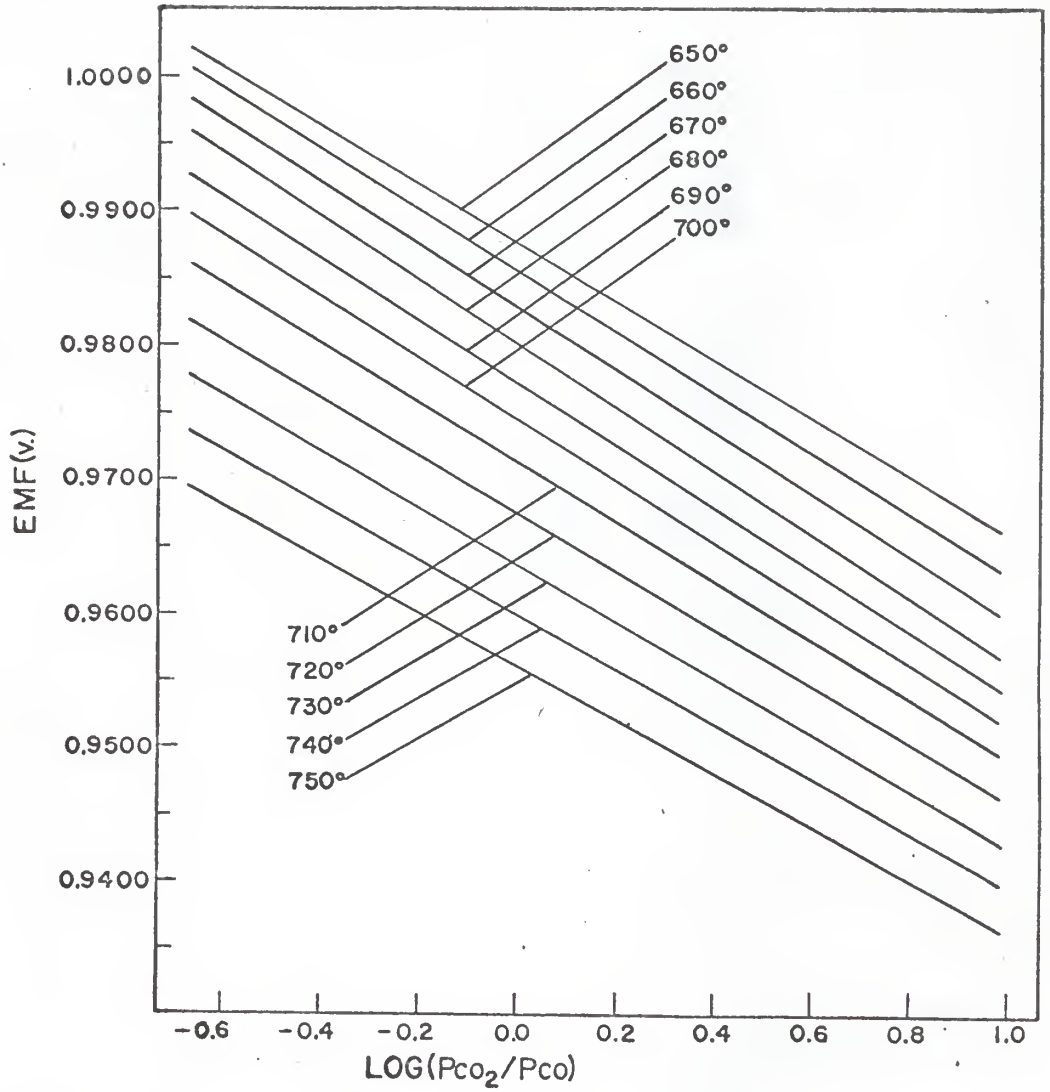

Figure 5. Experimental emf *vs.* common logarithm of the partial pressure ratios of CO_2 to CO, with the temperatures as indicated in °C.

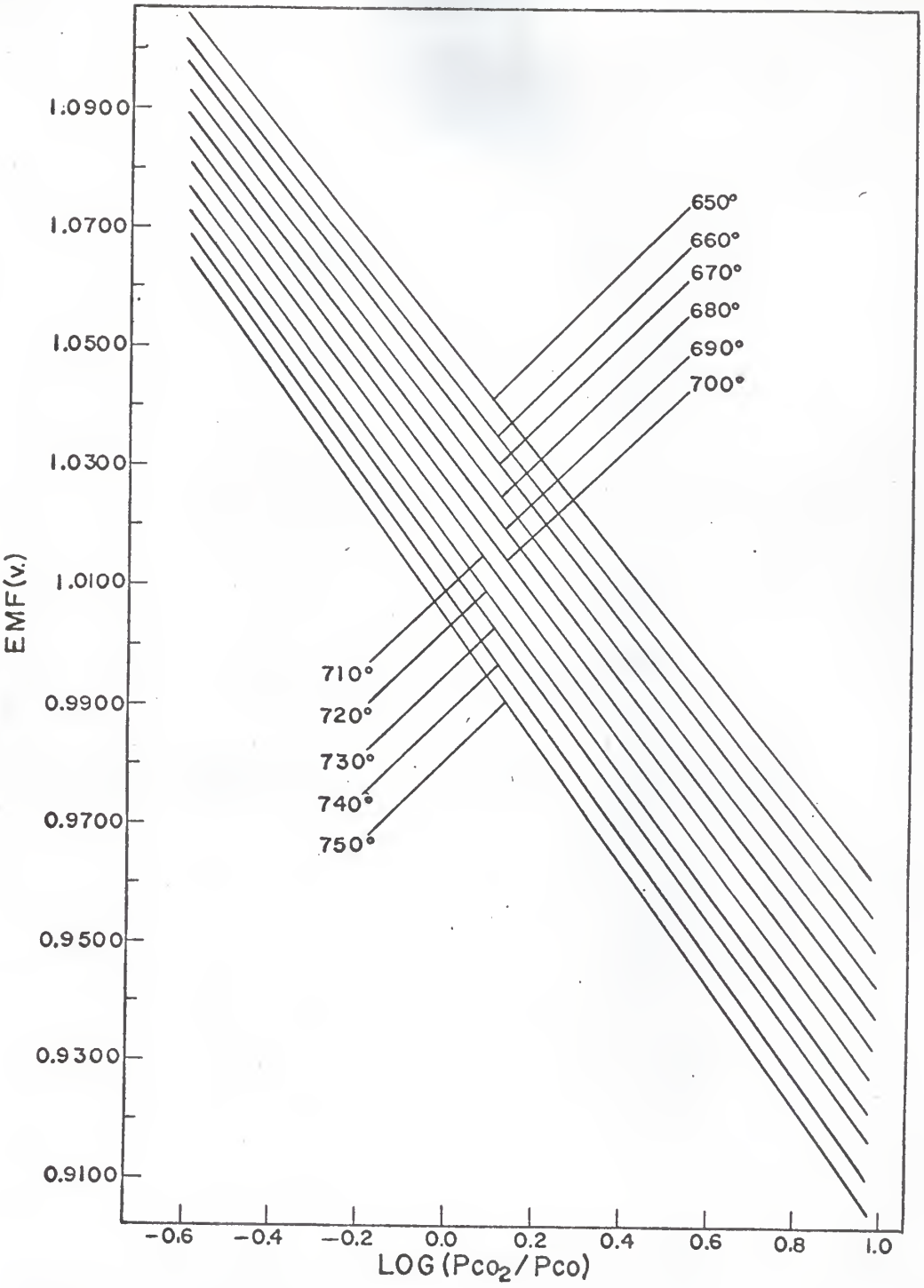

Figure 6. Theoretical emf vs. common logarithm of the partial pressure ratios of CO_2 to CO, with the temperatures as indicated in °C.

Table 12. Summary of slopes of emf *vs.* common logarithm of CO_2 to CO partial pressure ratio plots.

T (°C)	(-)Experimental Slope	(-)Theoretical Slope
650	0.0020	0.0916
660	0.0021	0.0926
670	0.0021	0.0936
680	0.0022	0.0946
690	0.0021	0.0956
700	0.0021	0.0966
710	0.0020	0.0975
720	0.0020	0.0985
730	0.0020	0.0995
740	0.0020	0.1005
750	0.0019	0.1015

DISCUSSION

It is apparent from the observed emf's and the plots in Fig. 3 and 5 that the electrode system behaved irreversibly. In studies performed by Duke and Copeland (1), involving the electrochemical oxidation of graphite in a molten sodium tungstate-tungstic anhydride electrolyte, the deviation of the observed from the theoretical emf was assumed to be affected by a local activity of CO_2, at the graphite electrode, greater than unity. The effect would be to lower the observed emf in accordance with eq 23. The local supersaturation of CO_2 was attributed to inability to agitate the electrolyte around the graphite electrode either by bubbling the gas or by some other action. This explanation does not seem reasonable for the present system, since it would always predict an observed emf less than the theoretical value. From Table 5 it is seen that the observed emf values are slightly larger than the theoretical values.

It would be presumptuous and mere speculation, on the basis of this study, to attempt any type of explanation for the deviation of the observed emf's from the theoretical values. Additional studies such as polarization studies, would have to be completed before attempting any explanation of what might be happening at the electrodes.

It can be concluded, however, that this system does appear to have potential possibilities as a fuel cell. The system was found to be rather stable and the observed emf's were quite reproducible. The molten polyphosphate system also affords several advantages over other molten electrolytes, such as the carbonates and mixtures of a salt and a corresponding oxide (e.g., sodium tungstate-tungstic anhydride). With the electrochemical oxidation of CO in a molten carbonate electrolyte, CO_2 must always be added along with the CO in order to regenerate the CO_3^{-2} ion (5). With electrolyte systems in

which an oxide (1, 2) is added to a salt, the problem of the oxide subliming out of the melt is encountered. The effect would be an ever-changing electrolytic system. With the molten polyphosphate electrolyte both of these problems are avoided. In addition, the unusually high corrosive nature of many molten salts is not a characteristic of the polyphosphate system. In conclusion it can be said that although this system appears to have potential possibilities as a fuel cell, much work still remains to be done to evaluate it fully.

ACKNOWLEDGMENTS

The author wishes to acknowledge the assistance and encouragement given to him by Dr. James L. Copeland during the course of this research.

A special acknowledgment is extended to Louann, the author's wife, for her continual patience and understanding.

The author also gratefully acknowledges support of this work by the National Science Foundation, Grant GP-7012 and by the Bureau of General Research, Kansas State University, Manhattan, Kansas.

REFERENCES

1. F. R. Duke and J. L. Copeland, U.S. Atomic Energy Commission, IS-665 (1963).
2. L. A. King and F. R. Duke, J. Phys. Chem., 68, 1536 (1964).
3. G. J. Young and R. B. Rozelle, J. Chem. Ed., 36, 68 (1959).
4. J. Weissbart, ibid., 38, 276 (1961).
5. K. R. Williams, in "An Introduction to Fuel Cells", K. R. Williams editor, Elsevier, New York, N. Y., 1966, pp. 1-13, 156-181.
6. W. R. Grove, Phil. Mag., 14, 127 (1839).
7. P. Jablockoff, Compt. Rend., 85, 1052 (1877).
8. W. W. Jacques, Z. Elektrochem., 4, 129 (1897).
9. F. Haber and R. Brunner, ibid., 10, 697 (1904).
10. A. Reed, Trans. Electrochem. Soc., 33, 89 (1918).
11. E. Baur and H. Ehrenburgh, Z. Elektrochem., 18, 1002 (1912).
12. E. Baur and H. Preis, ibid., 43, 727 (1937).
13. L. Mond and C. Langer, Proc. Roy. Soc., 46, 296 (1889).
14. R. Beutner, Z. Elektrochem., 17, 91 (1911).
15. H. H. Greger, U.S. Patent 2,175,523 (1939).
16. E. W. Junger, U.S. Patent 884,664 (1908).
17. E. N. Rideal and U. R. Evans, Trans. Faraday Soc., 17, 466 (1921-2).
18. E. Baur and T. Tobler, Z. Elektrochem., 39, 169 (1933).
19. F. T. Bacon, Chapter 5 in "Fuel Cells", G. J. Young editor, Vol. 1, Reinhold, New York, 1960.
20. F. Daniel, et. al., "Experimental Physical Chemistry", McGraw-Hill Book Co. Inc., New York, Chapters 2, 3, 9, and 22, (1962).
21. D. P. Shoemaker and C. W. Garland, "Experiments In Physical Chemistry", McGraw-Hill Book Co. Inc., New York, Chapters 5 and 8, (1962).
22. S. Glasstone, "Thermodynamic For Chemists", 2nd ed., D. Van Nostrand Co. Inc., New York, pp. 296-304, (1947).

23. S. Glasstone, "Introduction to Electrochemistry", 4th printing, D. Van Nostrand Co. Inc., New York, pp. 184-186, (1951).

24. G. N. Lewis and M. Randall, "Thermodynamics", 2nd ed., revised by K. S. Pitzer and L. Brewer, McGraw-Hill Book Co. Inc., New York, pp. 53-73 and 158-183, (1961)

25. "Handbook of Chemistry and Physics", Chemical Rubber Publishing Co., Cleveland, Ohio, 44th ed., p. e-85.

26. Kindly constructed by M. Ohno, Phys. Dept., Kansas State University, Manhattan, Kansas.

27. J. R. Van Wazer, "Phosphorus and Its Compounds", Interscience Publishers, Inc., New York, Vol. 1, p. 608.

28. K. K. Kelly, U. S. Bur. Mines Bull. 584.

STUDIES OF A HIGH TEMPERATURE $CO-O_2$ FUEL-TYPE CELL

by

LESLIE GUTIERREZ

B.S. Sioux Falls College, 1966

AN ABSTRACT OF A MASTER'S THESIS

submitted in partial fulfillment of the

requirements for the degree

MASTER OF SCIENCE

Department of Chemistry

KANSAS STATE UNIVERSITY
Manhattan, Kansas

1969

An electrochemical cell of the type: $CO(Pt)$; $Na_4P_2O_7$, $NaPO_3$; $(Pt)O_2$ has been studied with the objective of electrochemically determining thermodynamic properties associated with the high temperature formation of CO_2. The respective anode and cathode reactions are apparently:

anode: $CO(g) + P_2O_7^{-4} \rightarrow CO_2(g) + 2PO_3^- + 2e^-$

cathode: $1/2\ O_2(g) + 2PO_3^- + 2e^- \rightarrow P_2O_7^{-4}$

net reaction: $CO(g) + 1/2\ O_2(g) \rightarrow CO_2(g)$

Mixtures of CO and CO_2, at various partial pressure ratios, served as the anode and O_2 at 1 atm served as the cathode. The partial pressure ratios of CO_2 to CO studied were 0.258, 0.656, 1.00, 3.17, and 9.00, in addition to a run involving pure CO. These gases were introduced into separate wells of the cell which contained an electrolytic melt composed of 33 wt. % of $Na_4P_2O_7$. and 67 wt. % of $NaPO_3$; 24-gauge platinum wire served as electrical contacts and electrode substrates. The emfs produced by the cell at each partial pressure ratio of CO_2 to CO and O_2, as indicated above, were measured from 650 to 750°. The $\Delta\underline{G}$, $\Delta\underline{H}$, $\Delta\underline{S}$, and $\underline{K}$ (equilibrium constant) for the oxidation of CO to CO_2 were obtained in the usual way and compared to their theoretical values. Deviations of less than 10% from the theoretical were found for $\Delta\underline{G}$, with $\Delta\underline{S}$ possessing the largest deviation from its theoretical value (30 to 35%).

Although the cell was found to behave irreversibly it possesses interesting possibilities as a fuel cell.